



Research Paper

Co–Pd/BiVO₄: High-performance photocatalysts for the degradation of phenol under visible light irradiation

Kunfeng Zhang, Yuxi Liu*, Jiguang Deng*, Shaohua Xie, Xingtian Zhao, Jun Yang, Zhuo Han, Hongxing Dai*

Beijing Key Laboratory for Green Catalysis and Separation, Key Laboratory of Beijing on Regional Air Pollution Control, Laboratory of Catalysis Chemistry and Nanoscience, Department of Chemistry and Chemical Engineering, College of Environmental and Energy Engineering, Beijing University of Technology, Beijing 100124, China

ARTICLE INFO

Keywords:

Co–Pd bimetallic nanoparticle
Leaf-like bismuth vanadate
Supported noble metal photocatalyst
Photocatalytic phenol degradation
Photocatalytic degradation mechanism

ABSTRACT

Leaf-like monoclinic BiVO₄ and yCo_xPd/BiVO₄ (Co_xPd loading (y) = 0.060 – 0.092 wt%; Co/Pd molar ratio (x) = 0.26 – 1.70) photocatalysts were prepared using the hydrothermal and polyvinyl alcohol-protected reduction methods, respectively. The Co–Pd nanoparticles (NPs) with a size of 4–6 nm were well dispersed on the surface of leaf-like BiVO₄. The bimetallic Co–Pd-loaded BiVO₄ samples performed much better than the monometallic Co- or Pd-loaded counterpart, with the 0.062Co_{1.70}Pd/BiVO₄ sample showing the best photocatalytic performance (the time for 90% phenol removal was 3 h under visible light irradiation) and good photocatalytic stability. The pseudo-first-order reaction rate constants (0.4753 – 0.8367 h⁻¹) obtained over yCo_xPd/BiVO₄ were much higher than those (0.0619 – 0.3788 h⁻¹) obtained over BiVO₄, 0.058Co/BiVO₄, and 0.083Pd/BiVO₄, with the 0.062Co_{1.70}Pd/BiVO₄ sample possessing the highest rate constant. In-depth investigations of X-ray photoelectron spectroscopy, photoluminescence spectroscopy, and photoelectrochemical measurements reveal that high dispersion of bimetallic Co–Pd NPs increased the surface Pd⁰ and superoxide anion radical concentrations and suppressed the recombination of photoinduced electrons and holes (hence enhancing the photocatalytic activity of yCo_xPd/BiVO₄). The partial deactivation of the 0.062Co_{1.70}Pd/BiVO₄ sample after 15 h of three recycle tests was mainly due to the decrease in adsorbed oxygen species concentration. In addition, the possible photocatalytic phenol degradation mechanism over the 0.062Co_{1.70}Pd/BiVO₄ sample was also proposed. We believe that the BiVO₄-supported Co–Pd NPs have promising applications for the photocatalytic elimination of organic pollutants in wastewater.

1. Introduction

The prominent increase of organic pollutants emissions in wastewater is a giant threat to the global environment and human health. A variety of technologies for elimination of organic pollutants have been developed [1], in which photocatalytic oxidation is widely recognized as a promising technology that allows the conversion of pollutants into harmless with the aid of solar energy. Due to the poor visible-light responding ability, low efficiency, and high cost, however, most of the photocatalysts investigated so far cannot meet the practical application requirements. To overcome these drawbacks, a number of strategies (such as ion doping, precious metal modification, and constructing heterojunction [2–6]) have been developed in the past decades.

Deposition of noble metal(s) (e.g., Pt, Pd, Au, and Ag) on the surface of a semiconductor has been proven to an effective strategy to improve

the photocatalytic performance [7–9]. In this case, the photogenerated electrons could transfer from the support to the noble metal(s) under light illumination, and the photogenerated charge carriers involved in the oxidation and reduction of reactants in different locations. For instance, Xu et al. [8] prepared the M@TiO₂ (M = Au, Pd, and Pt) catalysts using a hydrothermal method, and observed that the loading of noble metal nanoparticles (NPs) enhanced the photocatalytic activity for the degradation of rhodamine B under visible light irradiation. Working on the preparation and photocatalytic activity of TiO₂ nanorod bundles-supported Au NPs for NO oxidation, Li and coworkers [10] pointed out that the photocatalytic activity over the supported Au NPs was about 3.4 times higher than that over pure TiO₂. Using a photo-reduction method, Meng et al. [11] synthesized the Pd-loaded rGO – Bi₂MoO₆ composites, and found that the supported Pd catalyst performed well in phenol decomposition, which was due to the increased visible light harvesting ability induced by the surface plasmonic

* Corresponding authors.

E-mail addresses: yxliu@bjut.edu.cn (Y. Liu), jgdeng@bjut.edu.cn (J. Deng), hxdai@bjut.edu.cn (H. Dai).

resonance effect.

Although these noble metal-decorated photocatalysts are effective for organic pollutants degradation, their photocatalytic activities are still not satisfactory and the used precious metals are expensive. In recent years, bimetallic NPs have been widely investigated in photocatalysis. For example, Sun et al. [12] examined the photocatalytic oxidation of benzyl alcohol over $\text{AuCu}@\text{CeO}_2$, and observed that catalytic activity and selectivity obtained over $\text{AuCu}@\text{CeO}_2$ were much higher than that obtained over the monometallic counterparts. These authors concluded that the enhanced photocatalytic activity was due to oxygen vacancies generated in CeO_2 and formation of an Au–Cu alloy. Moreover, the $\text{AuCu/SrTiO}_3/\text{TiO}_2$, AuPd/TiO_2 , and PdCu-TiO_2 photocatalysts [13–15] were also reported to show good photocatalytic performance.

Recently, the Bi-based semiconductor materials (e.g., Bi_2O_3 [16], BiOBr [17], BiVO_4 [18], BiPO_4 [19], Bi_2WO_6 [20], and Bi_2MoO_6 [21]) have attracted much attention. Among these developed materials, BiVO_4 has been the most intensively investigated in water splitting and environmental remediation due to its strong visible light responsibility, nontoxicity, and high stability [22]. However, a big problem of BiVO_4 is its undesirable charge carrier recombination and low conduction band position. To overcome this problem, many researchers developed and prepared noble metal-modified BiVO_4 (e.g., Au/BiVO_4 [23], Pd/BiVO_4 [24], and AuPd/BiVO_4 [25]) catalysts and found that they performed better than pure BiVO_4 .

Based on the literature [26,27], we believe that the Co and Pd atoms have an appropriate electronic match, and the photocatalytic efficiency could be enhanced if Pd is properly doped with Co to form a bimetal or alloy. Herein, we report for the first time the synthesis, characterization, and photocatalytic properties of leaf-like BiVO_4 -supported bimetallic Co–Pd NPs for the degradation of phenol under visible light irradiation. It is found that the 0.062 wt% $\text{Co}_{1.70}\text{Pd/BiVO}_4$ sample exhibited the excellent photocatalytic activity and stability. To the best of our knowledge, there have been no reports on the photocatalytic degradation of organic pollutants over the semiconductor-supported bimetallic (transition metal and noble metal) photocatalysts under visible light illumination. In the BiVO_4 -supported bimetallic Co–Pd photocatalysts, the introduction of Co to Pd could not only effectively promote the transfer of electrons from cobalt to palladium but also remarkably reduce the possibility in oxidation of Pd NPs, hence significantly improving the photocatalytic activity as compared with the monometallic Pd-loaded BiVO_4 photocatalyst. Moreover, in contrast to the supported double noble metal catalysts, the supported Co–Pd catalysts were also lower in cost. Therefore, our work offers a new route for the design of high-performance photocatalysts and their applications in the photocatalytic elimination of organic pollutants in wastewater.

2. Experimental

2.1. Preparation of leaf-like BiVO_4

The BiVO_4 support with a leaf-like morphology was prepared by the hydrothermal method described previously [28]. The typical synthesis procedures are as follows: Firstly, 4.851 g of $\text{Bi}(\text{NO}_3)_3 \cdot 5\text{H}_2\text{O}$ and 1.972 g of triblock copolymer (P123) were dissolved in 50 mL of HNO_3 aqueous solution (2.0 mol/L) under stirring. After being completely dissolved, 1.170 g of NH_4VO_3 was added to the above aqueous solution to obtain a transparent yellow solution. Afterwards, the pH of the mixed solution was adjusted to 9.0 with a $\text{NH}_3\text{-H}_2\text{O}$ aqueous solution (14 wt %). Finally, the resulting mixed solution (about 80 mL) was transferred into a 100-mL Teflon-lined stainless steel autoclave at 180 °C for 6 h. After being cooled to room temperature (RT), the solid was filtered and washed with deionized water and absolute ethanol three times, respectively. The sample was dried at 80 °C for 8 h and calcined in muffle furnace at a ramp of 1 °C/min from RT to 400 °C and maintained at this

temperature for 4 h, thus obtaining the leaf-like BiVO_4 support.

2.2. Preparation of $\text{Co}_x\text{Pd/BiVO}_4$, Co/BiVO_4 , and Pd/BiVO_4

The $y\text{Co}_x\text{Pd/BiVO}_4$ (theoretical Co_xPd loading (y) = 0.100 wt%; theoretical Co/Pd molar ratio (x) = 0.25, 1.0, and 2.0) were synthesized using the chemical reduction method with polyvinyl alcohol (PVA, MW = 10,000 g/mol) as protecting agent and NaBH_4 as reducing agent. In a typical procedure, a certain amount of PVA (1.00 mg/mL), CoCl_2 (0.10 mol/L), and PdCl_2 (0.10 mol/L) solution were mixed in a 50-mL flask and a N_2 environment under stirring. The total metal/PVA mass ratio was 1.00:1.50 and the theoretical Co_xPd loading was 0.100 wt%. After vigorous stirring in an ice bath for 10 min, a freshly prepared NaBH_4 aqueous solution (1.00 mg/mL; total metal/ NaBH_4 molar ratio = 1.00:5.00) was rapidly added to the above mixed aqueous solution for reduction of the metal ions to metal NPs. Then, a certain amount of the leaf-like BiVO_4 support was added to the suspension containing the Co_xPd NPs under stirring for 6 h. Afterwards, the wet solid was filtered and washed with deionized water and absolute ethanol three times, respectively. The $y\text{Co}_x\text{Pd/BiVO}_4$ photocatalysts were obtained after the solids being dried at 70 °C for 10 h and calcined in a tubular furnace and N_2 atmosphere at a ramp of 1 °C/min from RT to 200 °C and kept at this temperature for 1 h. For comparison, we also synthesized the $y\text{Co/BiVO}_4$ and $y\text{Pd/BiVO}_4$ samples using the above method in the absence of PdCl_2 and CoCl_2 aqueous solutions, respectively. The results (Table 1) of inductively coupled plasma atomic emission spectroscopic (ICP–AES) investigations reveal that the real Co_xPd loading (y) in $y\text{Co}_x\text{Pd/BiVO}_4$ was 0.092, 0.060, and 0.062 wt%, and the real Co/Pd molar ratio (x) in $y\text{Co}_x\text{Pd/BiVO}_4$ was 0.26, 0.90, and 1.70, respectively; the real Co loading (y) in $y\text{Co/BiVO}_4$ was 0.058 wt%, and the real Pd loading (y) was 0.083 wt% in $y\text{Pd/BiVO}_4$. The as-obtained photocatalysts are denoted as $0.092\text{Co}_{0.26}\text{Pd/BiVO}_4$, $0.060\text{Co}_{0.90}\text{Pd/BiVO}_4$, $0.062\text{Co}_{1.70}\text{Pd/BiVO}_4$, 0.058Co/BiVO_4 , and 0.083Pd/BiVO_4 , respectively.

All of the chemicals (A.R. in purity) were purchased from the Beijing Chemical Reagents Company and used without further purification.

2.3. Photocatalyst characterization

Physicochemical properties of the BiVO_4 , 0.058Co/BiVO_4 , 0.083Pd/BiVO_4 , and $y\text{Co}_x\text{Pd/BiVO}_4$ samples were characterized by ICP–AES, X-ray powder diffraction (XRD), scanning electron microscopy (SEM), transmission electron microscopy (TEM), high-angle annular dark field scanning transmission electron microscopy (HAADF–STEM), energy-dispersive X-ray (EDX) spectroscopic element mapping, N_2 adsorption–desorption (BET), UV-vis diffuse reflectance spectroscopy

Table 1

BET surface areas, average crystallite sizes (D_{BiVO_4}), real Co or Pd loadings, and real Co/Pd molar ratios of the samples.

Sample	BET surface area (m ² /g)	D_{BiVO_4} ^a (nm)	Real Co or Pd loading ^b (wt%)		Real Co/Pd molar ratio ^b
			Co	Pd	
BiVO_4	3.3	29	–	–	–
0.058Co/BiVO_4	3.5	28	0.058	–	–
0.083Pd/BiVO_4	3.6	28	–	0.083	–
$0.092\text{Co}_{0.26}\text{Pd/BiVO}_4$	3.4	30	0.011	0.081	0.26
$0.060\text{Co}_{0.90}\text{Pd/BiVO}_4$	3.6	29	0.020	0.040	0.90
$0.062\text{Co}_{1.70}\text{Pd/BiVO}_4$	3.5	29	0.032	0.030	1.70

^a Estimation according to the Scherrer equation using the FWHM of the (112) line of BiVO_4 .

^b Determined by the ICP–AES technique.

(UV-vis DRS), photoluminescence spectroscopy (PL), X-ray photoelectron spectroscopy (XPS), electron paramagnetic resonance (EPR), and photoelectrochemical (PEC) measurements. The detailed characterization procedures are described in the Supplementary material.

2.4. Photocatalytic activity evaluation

Photocatalytic activities of the as-prepared samples were measured in a quartz reactor (QO250, Beijing Changtuo Sci. & Tech. Co. Ltd.) for the degradation of phenol under visible light irradiation. In order to eliminate the effect of temperature shift on the activity, the whole photocatalytic process was carried out at RT using flowing cool water. A 300 W Xenon lamp with an optical cut-off filter (Beijing Zhongjiaojinyuan Technology Co. Ltd., $\lambda \geq 400$ nm) was used as the visible light source. In a typical photocatalytic process, 80 mg of the photocatalyst was dispersed in 100 mL of phenol aqueous solution (initial phenol concentration $C_0 = 0.2$ mmol/L). Before visible light illumination, the resulting suspension was ultrasonically treated for 10 min and then stirred in the dark for 1 h to allow the system to establish the adsorption–desorption equilibrium. An air flow of 30 mL/min was passed through the suspension. During the irradiation period, 3.5 mL of the suspension was collected at certain intervals, then centrifuged to remove the photocatalyst particles, and finally the solution was filtered through a 0.22 μm nylon66 membrane filter. The reactant (phenol) and products were analyzed on a high-performance liquid chromatography (HPLC, Shimadzu) with a SPD-20A UV-vis detector and a Shim-pack XR-ODS III reversed phase column (50 \times 2.0 mm, i. d. = 1.6 μm). The mobile phase was a mixture of methanol and water (volumetric ratio = 80:20) at a total flow rate of 0.4 mL/min. The sampled products were analyzed using an automatic sampler and the injection amount was 10 μL . Phenol and product concentrations (C_t) after a certain reaction time (t) were determined by the external standard method. The conversion $((C_0 - C_t)/C_0 \times 100\%)$ of phenol with respect to reaction time was used to evaluate the photocatalytic activity.

3. Results and discussion

3.1. Crystal phase composition and surface area

The XRD patterns of pure BiVO_4 and its supported Co, Pd, and Co_xPd samples are shown in Fig. 1. All of the samples exhibited characteristic diffraction peaks at $2\theta = 18.7^\circ, 19.0^\circ, 28.9^\circ, 30.5^\circ, 34.5^\circ, 35.2^\circ, 39.7^\circ, 42.4^\circ, 46.7^\circ, 47.2^\circ, 50.2^\circ, 53.2^\circ, 58.3^\circ$, and 59.4° , which corresponded to the (101), (011), (112), (040), (200), (020), (211), (015), (204), (024), (220), (116), (312), and (224) crystal planes of the monoclinic BiVO_4 phase (JCPDS PDF# 75-1867) [29]. The grain sizes of BiVO_4 in the samples were calculated according to the Scherrer equation, as summarized in Table 1. The grain sizes of BiVO_4 in the pure BiVO_4 and supported samples were in the range of 28–30 nm. No obvious diffraction peaks assignable to the other phases were observed due to the low loadings (< 0.100 wt%) of Co, Pd, and Co_xPd and their high dispersion on the surface of leaf-like BiVO_4 . This result indicates that loading of the metal NPs did not influence the crystal structure of BiVO_4 . The BET surface areas of the samples were in the range of 3.3–3.6 m^2/g (Table 1).

3.2. Morphology

Fig. 2 shows the SEM and TEM images of the samples. All of the samples contained the leaf-like BiVO_4 with the trunk and branch sizes being 4–15 and 0.5–2.0 μm , respectively. The lattice fringes with the interplanar spacing of 0.306 nm were clearly observed from the TEM images, which corresponded to the (112) crystal plane of monoclinic BiVO_4 . Due to the small sizes, low loadings, and close contrast between metal NPs and BiVO_4 , it is hard to distinguish the Co, Pd, and Co_xPd

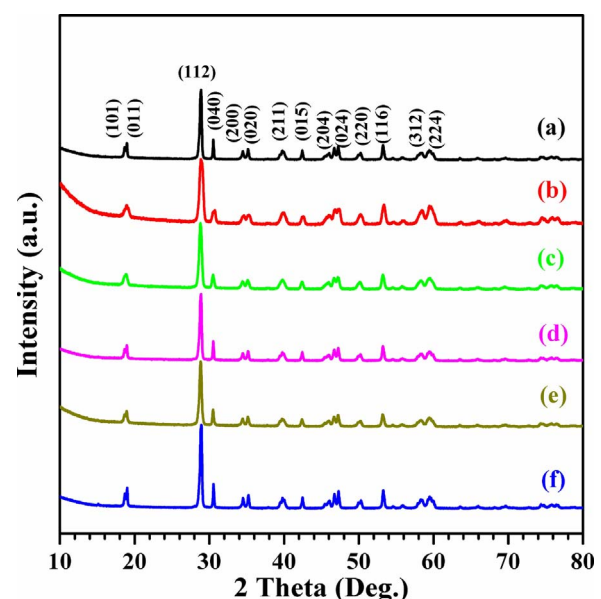


Fig. 1. XRD patterns of (a) BiVO_4 , (b) 0.058Co/ BiVO_4 , (c) 0.083Pd/ BiVO_4 , (d) 0.092Co_{0.26}Pd/ BiVO_4 , (e) 0.060Co_{0.90}Pd/ BiVO_4 , and (f) 0.062Co_{1.70}Pd/ BiVO_4 .

NPs from the BiVO_4 support. In order to confirm the existence and dispersion of metal NPs, the HAADF-STEM and EDX mapping characterizations were performed and their results are shown in Fig. 3. A number of bright dots were uniformly distributed on the surface of BiVO_4 , and the sizes of Co_{1.70}Pd NPs in Co_{1.70}Pd/ BiVO_4 were 4–7 nm. As shown in EDX mapping images, most of the Pd NPs were surrounded by Co NPs. This result confirms that the bimetallic Co–Pd NPs were formed in the 0.062Co_{1.70}Pd/ BiVO_4 sample. The synergistic effect between Co and Pd NPs might be favorable for the improvement in photocatalytic activity of the supported BiVO_4 samples.

3.3. Optical properties

Fig. 4 shows the UV-vis DRS and PL spectra of the samples. It is observed from Fig. 4A that all of the samples almost exhibited the same UV-vis DRS spectra, and the BiVO_4 -supported Pd and Co_xPd samples did not display enhanced absorption due to the extremely low Pd and Co_xPd loadings. The BiVO_4 sample possessed stronger absorption in the UV-vis region, with the maximal absorption wavelength extending to ca. 510 nm. According to the Kubelka-Munk equation ($ahv = A(hv - E_g)^{n/2}$ [30], where a is the absorption coefficient, hv is the photon energy, A is the constant, and n is equal to 1 (direct-gap semiconductor) or 4 (indirect-gap semiconductor)), the bandgap energies (E_g) of the samples were obtained from the extrapolated intercept on the abscissa axis (Fig. 4B). The E_g values of pure BiVO_4 , 0.058Co/ BiVO_4 , 0.083Pd/ BiVO_4 , 0.092Co_{0.26}Pd/ BiVO_4 , 0.060Co_{0.90}Pd/ BiVO_4 , and 0.062Co_{1.70}Pd/ BiVO_4 were 2.54, 2.55, 2.57, 2.58, 2.54, and 2.57 eV, respectively. The bandgap energy of a material represents the utilization efficiency of visible light, hence influencing its photocatalytic performance. The similar E_g values of the pure BiVO_4 and its supported Co, Pd, and Co_xPd samples suggest that light absorption was not an important factor in enhancement of photocatalytic activity of the samples obtained in the present work.

The recombination behaviors of photoinduced electrons and holes in the samples were measured by recording their steady-state PL spectra, as shown in Fig. 5. It is observed that all of the as-fabricated samples showed a similar emission peak with different intensity at wavelength = 390 nm. Compared to the pure BiVO_4 sample, the 0.058Co/ BiVO_4 and 0.083Pd/ BiVO_4 samples displayed a PL emission peak with a weaker intensity. The intensity of the PL emission peak could further be lower when Pd was doped with cobalt. Among the

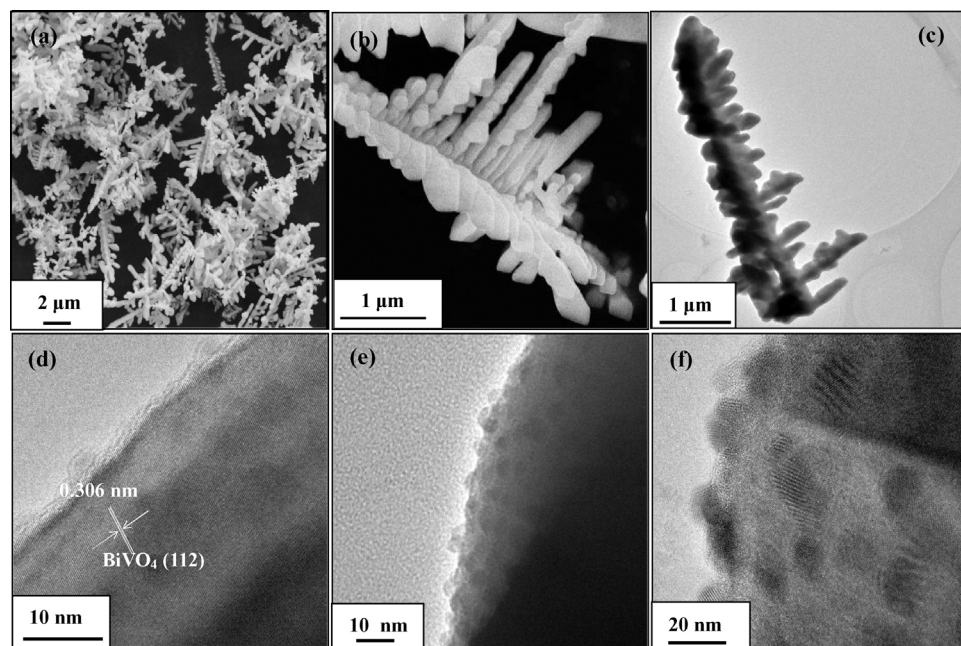


Fig. 2. (a, b) SEM and (c–f) TEM images of (a, c) BiVO_4 , (b, f) $0.062\text{Co}_{1.70}\text{Pd}/\text{BiVO}_4$, (d) $0.058\text{Co}/\text{BiVO}_4$, and (e) $0.083\text{Pd}/\text{BiVO}_4$.

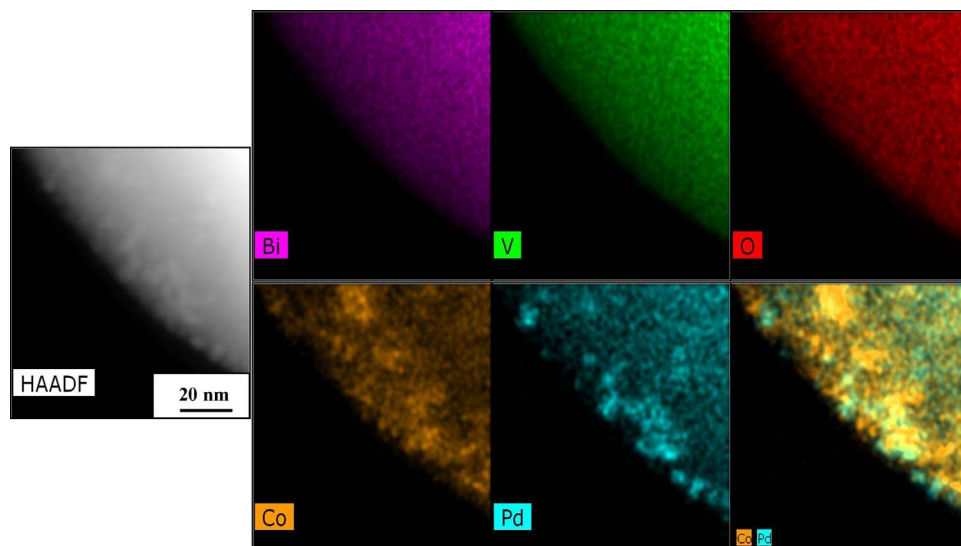


Fig. 3. HAADF-STEM images and EDX mapping of $0.062\text{Co}_{1.70}\text{Pd}/\text{BiVO}_4$.

$y\text{Co}_x\text{Pd}/\text{BiVO}_4$ samples, the $0.062\text{Co}_{1.70}\text{Pd}/\text{BiVO}_4$ sample showed a PL emission peak with the weakest intensity. It is generally accepted that the stronger intensity of a PL emission peak means the higher recombination probability of photogenerated electrons and holes, thus decreasing the photocatalytic activity of a sample [31–33]. Therefore, formation of bimetallic Co_xPd NPs could greatly inhibit the recombination of photoinduced charge carriers, as compared to the supported monometallic Pd or Co NPs.

3.4. Photocatalytic performance

Photocatalytic activities of the as-prepared samples were evaluated using phenol degradation under visible light irradiation, and the conversion of phenol versus reaction time is shown in Fig. 6. Due to the stability of phenol and the low surface areas ($< 4 \text{ m}^2/\text{g}$) of the samples, the conversion and adsorption of phenol were negligible in the absence of the photocatalysts under visible light irradiation and in the dark, respectively. Only 30% phenol was degraded over pure BiVO_4 after 5 h of visible light irradiation (Fig. 6). Unexpectedly, the conversion of

phenol became lower over the $0.058\text{Co}/\text{BiVO}_4$ sample. However, phenol conversion reached 85% over $0.083\text{Pd}/\text{BiVO}_4$ after 5 h of visible light illumination. It is generally accepted that deposition of precious metal(s) on the surface of a semiconductor can promote the transfer of photogenerated electrons from the semiconductor to the precious metal (s) until both the same Fermi levels are reached, thus effectively separating the photoinduced charge carriers [34]. Such a conclusion was further confirmed by the stronger photocurrent response and lower charge transfer resistance of the samples. The fast separation of photogenerated electrons and holes gave rise to improvement in phenol conversion over $0.083\text{Pd}/\text{BiVO}_4$. Interestingly, the $y\text{Co}_x\text{Pd}/\text{BiVO}_4$ photocatalysts at similar Pd loadings showed a dramatic synergistic effect of Co and Pd on improvement in photocatalytic efficiency for phenol degradation. $y\text{Co}_x\text{Pd}/\text{BiVO}_4$ were superior to $0.083\text{Pd}/\text{BiVO}_4$ in terms of photocatalytic phenol degradation, and the activity increased with the rise in Co content. The $0.060\text{Co}_{1.70}\text{Pd}/\text{BiVO}_4$ sample exhibited the best photocatalytic activity, with the reaction time for 90% phenol removal being 3 h. Taking into account the results of EDX mapping and PL characterizations, we conclude that the excellent photocatalytic

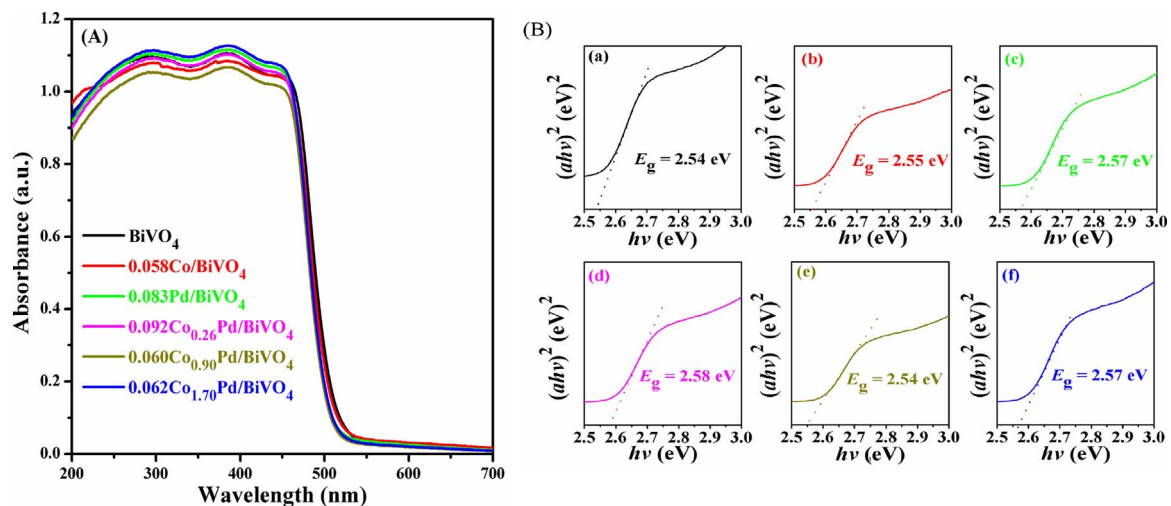


Fig. 4. (A) UV-vis diffuse reflectance spectra and (B) $(ahv)^2$ versus $h\nu$ plots of (a) BiVO₄, (b) 0.058Co/BiVO₄, (c) 0.083Pd/BiVO₄, (d) 0.092Co_{0.26}Pd/BiVO₄, (e) 0.060Co_{0.90}Pd/BiVO₄, and (f) 0.062Co_{1.70}Pd/BiVO₄.

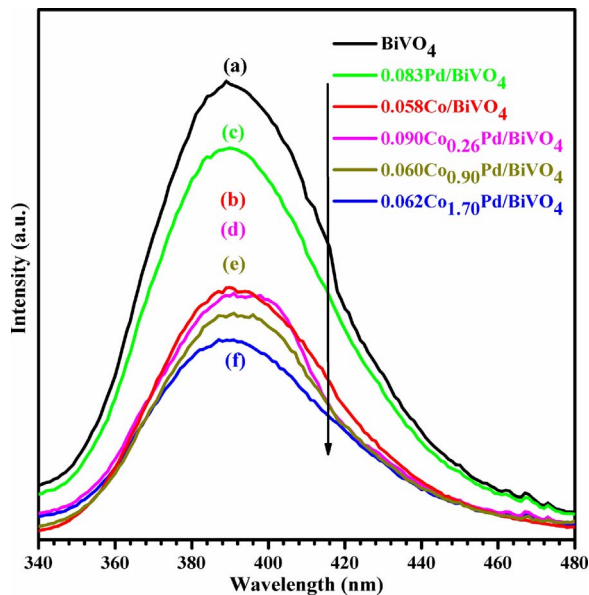


Fig. 5. Photoluminescence spectra of (a) BiVO₄, (b) 0.058Co/BiVO₄, (c) 0.083Pd/BiVO₄, (d) 0.092Co_{0.26}Pd/BiVO₄, (e) 0.060Co_{0.90}Pd/BiVO₄, and (f) 0.062Co_{1.70}Pd/BiVO₄.

activity of 0.060Co_{1.70}Pd/BiVO₄ was associated with high dispersion bimetallic Co–Pd NPs and low recombination of photoinduced charge carriers.

In order to clearly compare the photocatalytic activities, we investigated the photocatalytic phenol degradation kinetics over the samples. As shown in Fig. 7, the degradation of phenol fitted a pseudo-first-order kinetic model. The reaction kinetics equation is as follows [35,36]:

$$-\ln(C_t/C_0) = k t$$

where C_t , C_0 , k , and t are the phenol concentration after a certain reaction time (t), initial phenol concentration, apparent rate constant (h^{-1}), and reaction time, respectively. The k value and correlation coefficient (R^2) are summarized in Table 2. It is found that the model was suitable for describing the photocatalytic phenol degradation processes. The rate constant (0.8367 h^{-1}) over the 0.062Co_{1.70}Pd/BiVO₄ sample was the highest, which was ca. 14 and 2.2 times higher than those (0.0619 and 0.3788 h^{-1}) over the pure BiVO₄ and 0.083Pd/BiVO₄ samples, respectively.

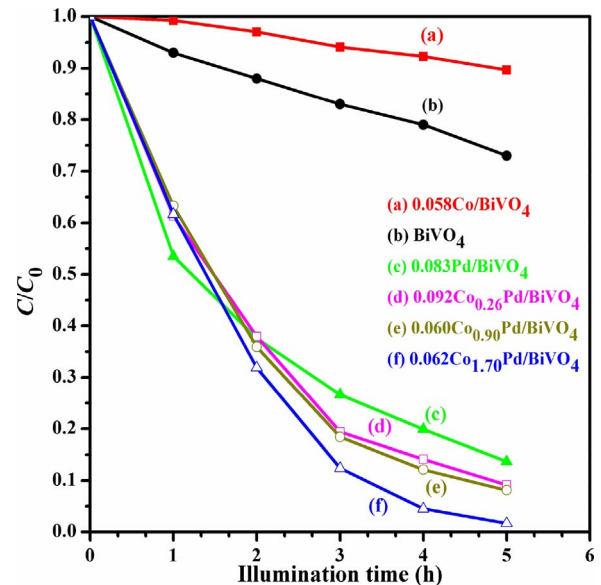


Fig. 6. Phenol concentration versus visible light illumination time over (a) BiVO₄, (b) 0.058Co/BiVO₄, (c) 0.083Pd/BiVO₄, (d) 0.092Co_{0.26}Pd/BiVO₄, (e) 0.060Co_{0.90}Pd/BiVO₄, and (f) 0.062Co_{1.70}Pd/BiVO₄ for the degradation of phenol aqueous solution ($C_0 = 0.2 \text{ mmol/L}$) under visible light ($\lambda \geq 400 \text{ nm}$) illumination.

Recycling photocatalytic activity tests were conducted to evaluate the stability of the 0.062Co_{1.70}Pd/BiVO₄ sample under the same reaction conditions, and their results are shown in Fig. 8. Obviously, phenol conversion slightly decreased after 15 h of three recycle tests, and 80% phenol conversion was maintained. In order to investigate the reason why the photocatalytic activity decreased after three recycle tests, we conducted the XRD and XPS characterization of the used 0.062Co_{1.70}Pd/BiVO₄ sample, and the results are shown in Figs. S1 and S2, respectively. It can be seen from Fig. S1 that there were no significant changes in characteristic diffraction peaks of the fresh and used 0.062Co_{1.70}Pd/BiVO₄ samples, indicating that the crystal structure of the 0.062Co_{1.70}Pd/BiVO₄ photocatalyst was not altered after 15 h of recycle tests. That is to say, the partial deactivation of this catalyst was not due to the change in crystal structure. It can be observed from Fig. S2 that the Bi 4f, V 2p, and Co 2p_{3/2} XPS spectra of the fresh and used 0.062Co_{1.70}Pd/BiVO₄ samples were almost unchanged. However, there was a significant alteration in the O 1s or Pd 3d XPS spectra of the used samples after 15 h of recycle tests. The Pd⁰/Pd²⁺ and O_{ads}/O_{latt} molar

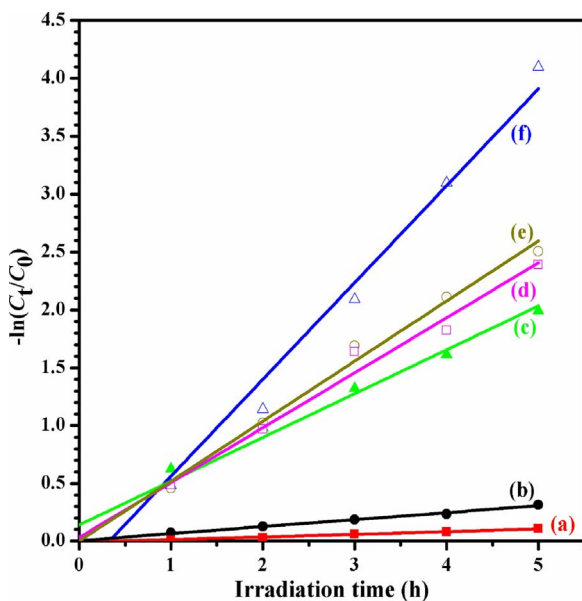


Fig. 7. Kinetic curves obtained over (a) 0.058Co/BiVO₄, (b) BiVO₄, (c) 0.083Pd/BiVO₄, (d) 0.092Co_{0.26}Pd/BiVO₄, (e) 0.060Co_{0.90}Pd/BiVO₄, and (f) 0.062Co_{1.70}Pd/BiVO₄ for phenol ($C_0 = 0.2$ mmol/L) degradation under visible light irradiation.

Table 2

Surface element compositions, bandgap energies (E_g), rate constants (k), and correlation coefficients (R^2) of the samples.

Sample	Surface element composition		E_g (eV)	k (min ⁻¹)	R^2
	V ⁴⁺ / V ⁵⁺	Pd ⁰ / Pd ²⁺	O _{ads} / O _{latt}		
	molar ratio	molar ratio	molar ratio		
BiVO ₄	0.031	–	0.42	2.54	0.0619
0.058Co/BiVO ₄	0.042	–	0.30	2.55	0.0227
0.083Pd/BiVO ₄	0.055	1.05	0.35	2.57	0.3788
0.092Co _{0.26} Pd/ BiVO ₄	0.064	1.48	0.45	2.54	0.4753
0.060Co _{0.90} Pd/ BiVO ₄	0.049	1.96	0.50	2.58	0.5190
0.062Co _{1.70} Pd/ BiVO ₄	0.045	2.41	0.53	2.57	0.8367

ratios decreased from 2.41 and 0.53–1.65 and 0.45, respectively. It is well known that O₂ molecules are usually adsorbed on the Pd⁰ site. The decrease in Pd⁰ content means the drop in adsorbed oxygen (e.g., O₂[–]) species concentration. Therefore, the partial deactivation of the 0.062Co_{1.70}Pd/BiVO₄ sample was associated with the decrease in adsorbed oxygen species concentration. Meanwhile, the slight decline in phenol conversion might also be due to the partial occupation of the active sites by the adsorption of intermediates and the inevitable partial loss of the photocatalyst during the recycling test processes [37].

3.5. Surface elemental composition, metal oxidation state, and adsorbed oxygen species

XPS characterization was conducted to investigate the surface element compositions, metal oxidation states, and adsorbed oxygen species of the samples. Fig. 9 shows the Bi 4f, V 2p, O 1s, Co 2p_{3/2}, and Pd 3d XPS spectra of the samples. From Fig. 9A, one can see the two symmetric peaks of characteristic Bi³⁺ species at binding energy (BE) = 159.0–159.3 and 164.3–164.6 eV that were assignable to the Bi 4f_{7/2} and Bi 4f_{5/2} signals, respectively. The XPS peaks in the V 2p_{3/2} and V 2p_{1/2} spectra at BE = 516.4–516.8 and 524.3–524.5 eV (Fig. 9B) could be attributed to the surface V⁵⁺ species [38]. The asymmetric O 1s XPS

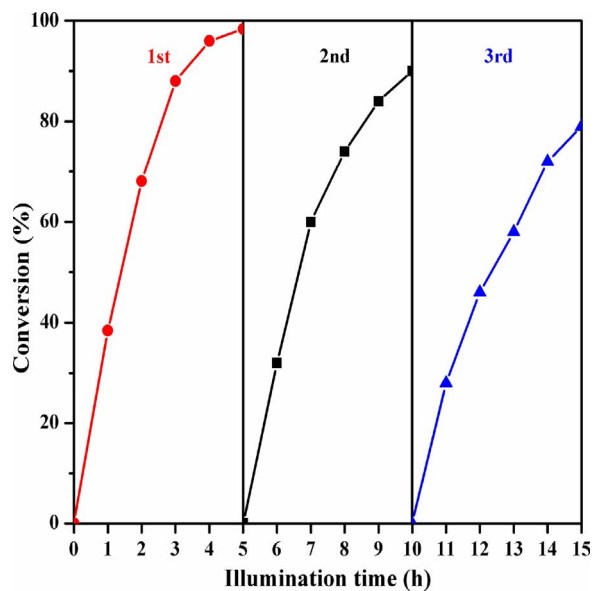


Fig. 8. Recycling tests of 0.062Co_{1.70}Pd/BiVO₄ for phenol ($C_0 = 0.2$ mmol/L) degradation under visible light irradiation.

signals could be decomposed into three components at BE = 529.6, 531.2, and 533.2 eV (Fig. 9C), which were ascribed to the surface lattice oxygen (O_{latt}), adsorbed oxygen (O_{ads}), and adsorbed water species [38,39], respectively. Fig. 9D shows the Co 2p_{3/2} XPS spectra of the 0.058Co/BiVO₄ and yCo_xPd/BiVO₄ samples. Due to the low Co loading, the Co 2p_{3/2} XPS signal is very poor. There was only the characteristic peak (at BE = 781.2 eV) assignable to the surface Co²⁺ species, and no apparent peaks could be ascribable to the surface metallic Co⁰ and Co³⁺ species [40]. In view of the poor photocatalytic activity of 0.058Co/BiVO₄ and excellent photocatalytic activity of Co₃O₄/BiVO₄ [41] for phenol degradation, we conclude that the Co on the surface of the BiVO₄ support was mainly Co²⁺ species (i.e., CoO). The Pd 3d XPS spectra of the 0.083Pd/BiVO₄ and yCo_xPd/BiVO₄ samples are shown in Fig. 9E. Each of the Pd 3d spectra could be decomposed into four components. The components at BE = 335.6 and 340.6 eV were assigned to the surface Pd⁰ species, whereas the ones at BE = 338.1 and 343.3 eV were attributed to the surface Pd²⁺ species [42]. The surface Pd⁰/Pd²⁺ and O_{ads}/O_{latt} molar ratios were calculated, as summarized in Table 2. Apparently, the order in photocatalytic activity of the samples was in good agreement with the sequence in Pd⁰/Pd²⁺ or O_{ads}/O_{latt} molar ratio. According to the literature [12,43], high metallic Pd⁰ and O_{ads} concentrations were beneficial for the catalytic process. Therefore, the 0.062Co_{1.70}Pd/BiVO₄ sample with the highest O_{ads} and Pd⁰ species concentrations showed the best photocatalytic activity for phenol degradation. Moreover, the doping of Co to Pd was favorable for the transfer of electrons from cobalt to palladium, leading to formation of bimetallic Co–Pd NPs. Therefore, the Co doping could effectively stabilize the metallic Pd⁰ species, giving rise to an increase in surface Pd⁰ species concentration (Table 2). Similar results were also reported by Sun et al. [12] who investigated the AuCu@CeO₂ catalyst system for photocatalytic oxidation of benzyl alcohol, in which the authors claimed the transfer of electrons from copper to gold.

3.6. Photoelectrochemical behavior

To further confirm the generation, transfer, and separation processes of the photoinduced electrons and holes, transient photocurrent density and electrochemical impedance spectra were measured over the as-prepared samples, and the results are shown in Fig. 10. The photocurrent experiments were carried out with the visible light switching on and off every 30 s [44]. As shown in Fig. 10A, the photocurrent density

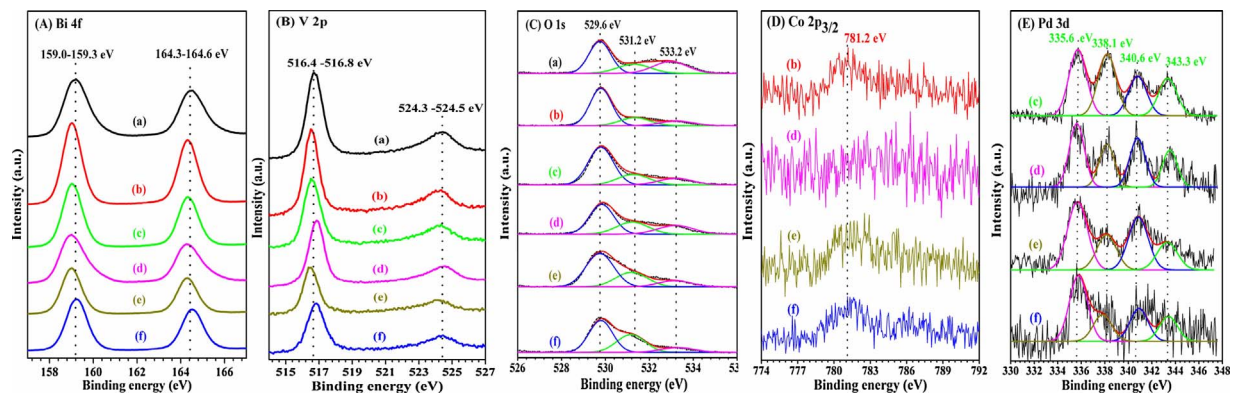


Fig. 9. (A) Bi 4f, (B) V 2p, (C) O 1s, (D) Co 2p_{3/2}, and (E) Pd 3d XPS spectra of (a) BiVO₄, (b) 0.058Co/BiVO₄, (c) 0.083Pd/BiVO₄, (d) 0.092Co_{0.26}Pd/BiVO₄, (e) 0.060Co_{0.90}Pd/BiVO₄, and (f) 0.062Co_{1.70}Pd/BiVO₄.

increased in the order of BiVO₄ < 0.083Pd/BiVO₄ < 0.092Co_{0.26}Pd/BiVO₄ < 0.058Co/BiVO₄ < 0.060Co_{0.90}Pd/BiVO₄ < 0.062Co_{1.70}Pd/BiVO₄, which was in agreement with the sequence in photocatalytic activity (except for 0.058Co/BiVO₄). According to the lower PL intensity and stronger photocurrent response of 0.058Co/BiVO₄, one can deduce that Co NPs supported on BiVO₄ would favor the separation and transfer of charge carriers [45,46], but the energy band structures might not match between Co NPs and phenol molecules [47] in the present work. The main reason why the 0.058Co/BiVO₄ sample showed the lowest photocatalytic activity might be the lowest O_{ads} species concentration. The 0.062Co_{1.70}Pd/BiVO₄ electrode possessed the highest photocurrent density, which was ca. 6 and 5 times higher than those of the BiVO₄ and 0.083Pd/BiVO₄ electrodes, respectively. The results confirm that the separation efficiency of the photogenerated charge carriers was improved by the loading of bimetallic Co–Pd NPs [48,49]. Furthermore, electrochemical impedance spectroscopic (EIS) measurements of the samples was conducted (0.7 V vs. Ag/AgCl, visible light) to investigate the charge transfer resistance [50]. The EIS Nyquist plots of the samples are shown in Fig. 10B. The Z' represents the real part of measured impedance, whereas the –Z'' represents the negative number of the imaginary part of measured impedance. In the EIS analysis, the arc radius reflects the charge transfer resistance between the semiconductor and electrolyte interface. Usually, a small radius in the EIS Nyquist plot means an efficient separation of the photogenerated electrons and holes and a fast mobility of photoinduced electrons [51,52]. Obviously, the radius was the smallest for 0.062Co_{1.70}Pd/BiVO₄ (Fig. 10B), indicative of the lowest

charge transfer resistance. Therefore, the 0.062Co_{1.70}Pd/BiVO₄ sample exhibited the lowest recombination probability and the fastest separation rate of the photogenerated charge carriers.

3.7. Photocatalytic degradation mechanism

The reactive species trapping experiments and degradation intermediates analysis were carried out to explore the possible photocatalytic mechanisms over the 0.062Co_{1.70}Pd/BiVO₄ sample. In order to determine the roles of the photogenerated reactive species during the photocatalytic phenol degradation processes, silver nitrate (0.01 mol/L), ammonium oxalate (AO, 0.01 mol/L), isopropyl alcohol (IPA, 0.01 mol/L), and benzoquinone (BQ, 0.01 mmol/L) were used as scavengers of the photogenerated electrons (e[−]), holes (h⁺), hydroxyl radicals (·OH), and superoxide anion radicals (O₂·[−]) [53,54], respectively, and the results are shown in Fig. 11. It can be observed that different scavengers had important effects on photocatalytic efficiency of the 0.062Co_{1.70}Pd/BiVO₄ sample. Phenol conversion slightly decreased with the addition of AgNO₃ or IPA. In contrast, phenol conversion significantly dropped from 98 to 34 and 30% within 5 h of visible light illumination when BQ and AO were added to the phenol aqueous solution, respectively. The results of the reactive species trapping experiments indicate that the photogenerated e[−] and ·OH were not the reactive species for photocatalytic phenol degradation, but the photocatalytic process might be mainly governed by the O₂·[−] and photogenerated h⁺.

In order to further validate the role of superoxide anion (O₂·[−])

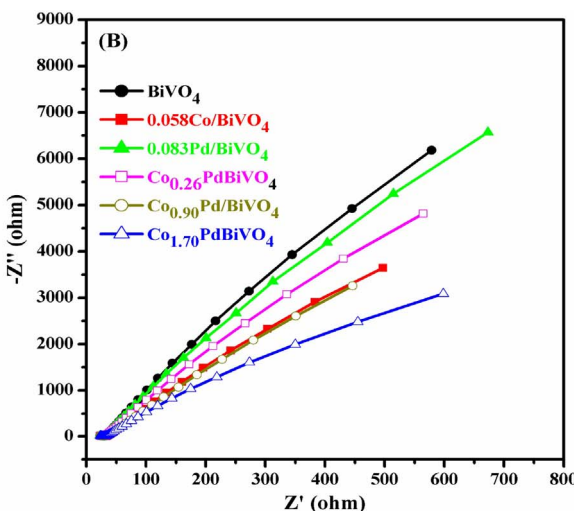
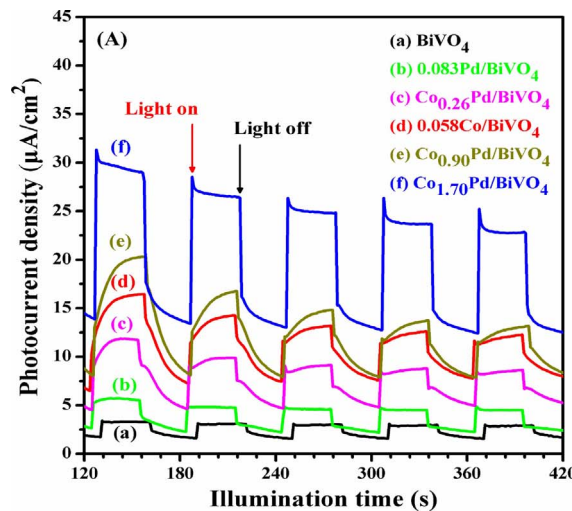


Fig. 10. (A) Transient photocurrent density with light on/off cycles and (B) EIS Nyquist plot measured at 0.7 V (vs. Ag/AgCl) over the samples in 0.5 mol/L Na₂SO₄ aqueous solution under visible light illumination ($\lambda \geq 400$ nm).

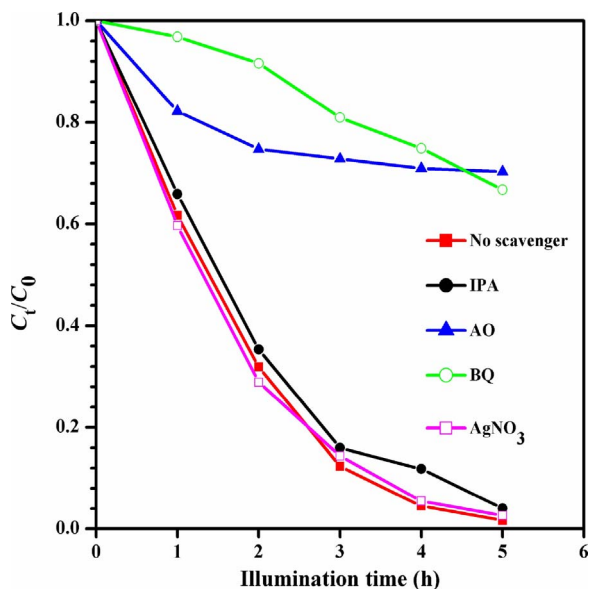


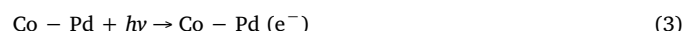
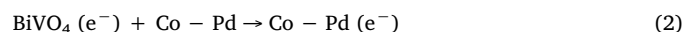
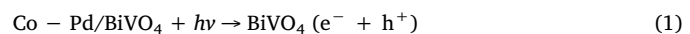
Fig. 11. Photocatalytic degradation of phenol over $0.062\text{Co}_{1.70}\text{Pd}/\text{BiVO}_4$ in the presence of isopropyl alcohol (IPA, 0.01 mol/L), ammonium oxalate (AO, 0.01 mol/L), benzoquinone (BQ, 0.01 mmol/L), and silver nitrate (AgNO_3 , 0.01 mol/L) under visible light irradiation.

radicals in photocatalytic process, we used the EPR technique to directly detect the reactive oxygen species. 5,5-dimethyl-1-pyrroline *N*-oxide (DMPO) was utilized as a radical trapping reagent to capture the $\cdot\text{OH}$ and $\text{O}_2^{\cdot-}$ radicals. It can be seen from Fig. 12 that under the irradiation of visible light from 3 to 10 min, there were no significant EPR signals over the pure BiVO_4 sample; very weak EPR signals were detected over the $0.083\text{Pd}/\text{BiVO}_4$ sample, indicating that there was a small amount of the $\cdot\text{OH}$ and $\text{O}_2^{\cdot-}$ species generated over the $0.083\text{Pd}/\text{BiVO}_4$ sample after visible light irradiation; however, the signal intensity of the $\cdot\text{OH}$ and $\text{O}_2^{\cdot-}$ species significantly increased over the $0.062\text{Co}_{1.70}\text{Pd}/\text{BiVO}_4$ sample, indicating that there was a high amount of the $\cdot\text{OH}$ and $\text{O}_2^{\cdot-}$ species formed over the $0.062\text{Co}_{1.70}\text{Pd}/\text{BiVO}_4$ sample. Considering the results of the reactive species trapping experiments (Fig. 11) and EPR characterization (Fig. 12), we believe that the photocatalytic process over the $0.062\text{Co}_{1.70}\text{Pd}/\text{BiVO}_4$ sample

was mainly governed by the $\text{O}_2^{\cdot-}$ and photogenerated h^+ .

The initial phenol and possible intermediates produced during the photocatalytic phenol degradation processes were detected by the HPLC. Fig. 13 shows the chromatograms of reaction products over the $0.083\text{Pd}/\text{BiVO}_4$ and $0.062\text{Co}_{1.70}\text{Pd}/\text{BiVO}_4$ samples. In addition to phenol, three reaction intermediates (hydroquinone, benzoquinone, and catechol) were detected, corresponding to the retention time of 3.53, 0.84, 1.25, and 1.70 min. It should be pointed out that the photocatalytic phenol degradation over the $0.083\text{Pd}/\text{BiVO}_4$ and $0.062\text{Co}_{1.70}\text{Pd}/\text{BiVO}_4$ samples was similar, and the evolution of phenol and intermediates was shown in Fig. 14. Apparently, phenol concentration quickly decreased; an accumulation of hydroquinone and benzoquinone was observed at the early stage of reaction, and then hydroquinone and benzoquinone concentrations slightly decreased with the extension of visible light irradiation time. However, the catechol concentration was rather low and not changed obviously during the whole reaction process. The maximal hydroquinone and benzoquinone concentrations over $0.083\text{Pd}/\text{BiVO}_4$ reached 9.4 and 9.7 $\mu\text{mol}/\text{L}$, whereas those over $0.062\text{Co}_{1.70}\text{Pd}/\text{BiVO}_4$ were 17.3 and 16.8 $\mu\text{mol}/\text{L}$, respectively. Hutchings and coworkers [14] also reported similar results over AuPd/TiO_2 for the degradation of phenol.

Based on the above results and those reported in the literature, we propose the possible photocatalytic mechanism of phenol degradation over the $0.062\text{Co}_{1.70}\text{Pd}/\text{BiVO}_4$ sample, as illustrated in Fig. 15. The possible photocatalytic processes are as follows:



Firstly, the electrons (e^-) in valence band of BiVO_4 under visible light illumination can be excited to the conduction band, leaving the holes (h^+) in valence band of BiVO_4 (Eq. (1)). After loading of the Co-Pd NPs, the photogenerated electrons in conduction band of BiVO_4 could be continually transferred to the Co-Pd NPs until the same Fermi levels reached since the work functions of metals were higher than that

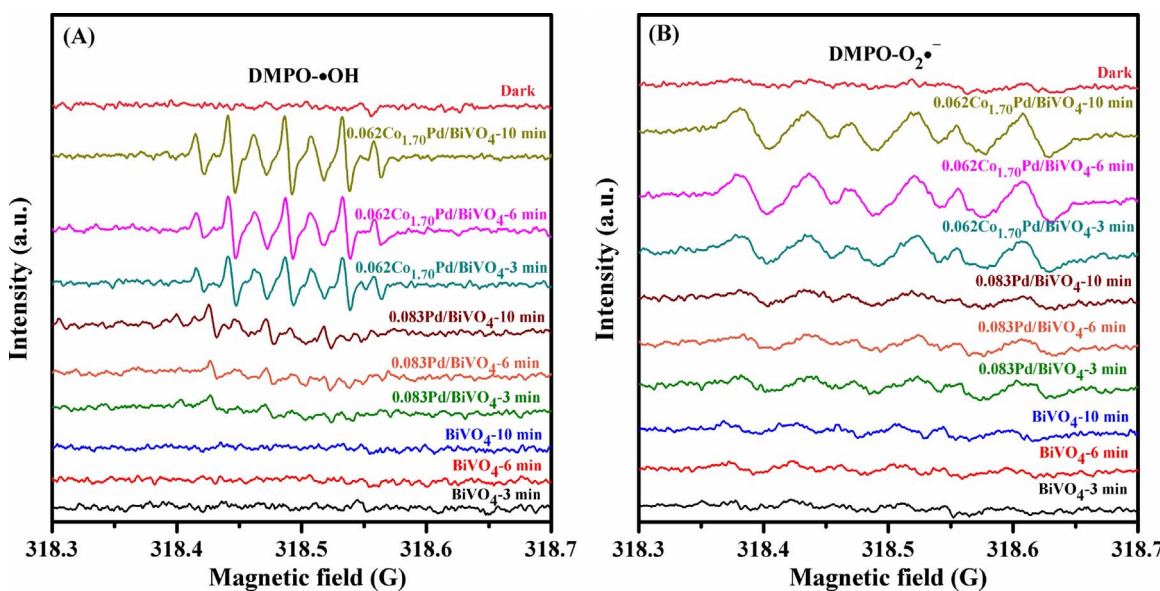


Fig. 12. EPR spectra of (A) DMPO - $\cdot\text{OH}$ and (B) DMPO - $\text{O}_2^{\cdot-}$ over the BiVO_4 , $0.083\text{Pd}/\text{BiVO}_4$, and $0.062\text{Co}_{1.70}\text{Pd}/\text{BiVO}_4$ samples in darkness and under visible light irradiation for 3, 6, and 10 min, respectively.

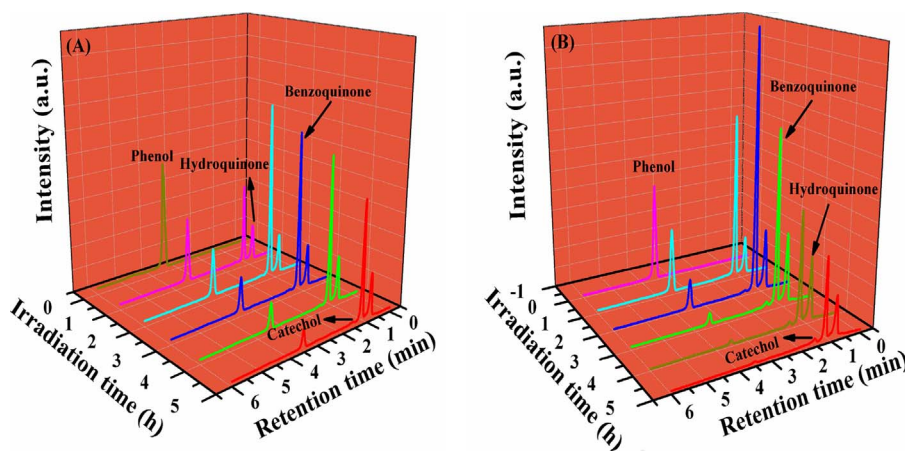


Fig. 13. HPLC chromatograms of phenol degradation over (A) 0.083Pd/BiVO₄ and (B) 0.062Co_{1.70}Pd/BiVO₄ under visible light irradiation.

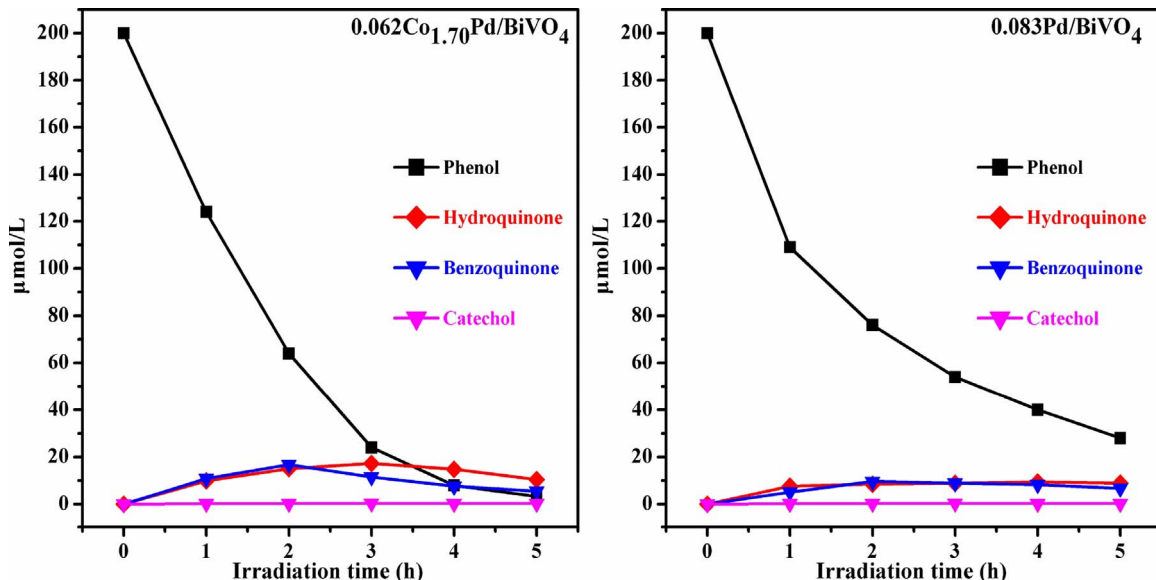


Fig. 14. Temporal evolution of phenol and intermediates 0.062Co_{1.70}Pd/BiVO₄ over and 0.083Pd/BiVO₄ under visible light irradiation.

of BiVO₄ (Eq. (2)). Thus, the photogenerated electrons and holes were located at Co-Pd NPs and BiVO₄, respectively, leading to the effective separation of the photoinduced charge carriers. Furthermore, the

electrons also might be generated from the Co-Pd NPs (Eq. (3)), which could easily react with the adsorbed oxygen molecules to produce superoxide anion radicals (O₂^{·-}) that could oxidize phenol to the

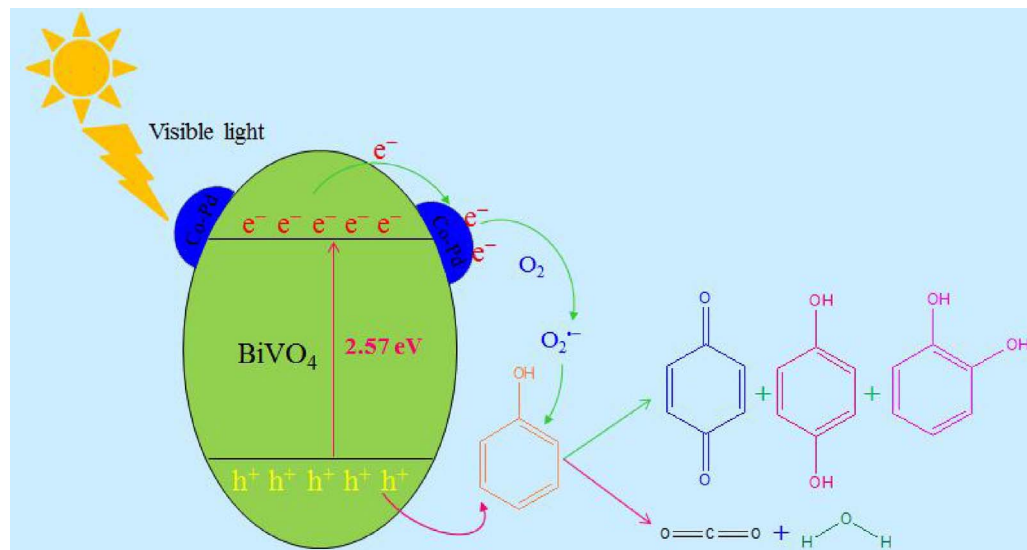


Fig. 15. Schematic illustration of the possible photocatalytic phenol degradation mechanism over the 0.062Co_{1.70}Pd/BiVO₄ photocatalyst under visible light irradiation.

products (Eqs. (4) and (5)). It should be pointed out that the possibility of O_2^- production from O_2 molecules induced by the electrons in the $BiVO_4$ support was rather low because of its low conduction band location according to our previous work [29], as confirmed by the EPR result of the pure $BiVO_4$ sample (Fig. 12). In the meanwhile, the photogenerated holes as strong oxidant could directly oxidize phenol to the products (Eq. (6)).

4. Conclusions

The leaf-like monoclinic $BiVO_4$ and its supported metal (Co, Pd, Co–Pd) NPs were synthesized using the hydrothermal and PVA-protected chemical reduction methods, respectively. The metal NPs with a size of 4–6 nm were well dispersed on the surface of $BiVO_4$. The photocatalytic activities over the $yCo_xPd/BiVO_4$ samples were much higher than those over the $BiVO_4$, 0.058Co/ $BiVO_4$, and 0.083Pd/ $BiVO_4$ samples, with the 0.062Co_{1.70}Pd/ $BiVO_4$ sample performing the best for phenol degradation under visible light illumination (the time for 90% phenol removal was 3 h at an initial phenol concentration of 0.2 mmol/L). The reactive species trapping experiments reveal that phenol degradation process was governed by the superoxide anions radical and photoinduced holes. The partial deactivation of the 0.062Co_{1.70}Pd/ $BiVO_4$ sample after 15 h of three recycle tests was mainly due to the decrease in adsorbed oxygen species concentration. Based on the results of PL, XPS, photocurrent response, and electrochemical impedance spectroscopic characterizations, we proposed the possible photocatalytic phenol degradation mechanism. It is concluded that the excellent photocatalytic activity of 0.062Co_{1.70}Pd/ $BiVO_4$ was associated with the generation of highly active superoxide anion radicals and photoinduced holes and good separation efficiency of the photo-generated charge carriers. We believe that the Co–Pd NPs-loaded $BiVO_4$ materials are promising photocatalysts in the oxidative removal of organic pollutants in wastewater.

Acknowledgements

This work was supported by the NSF of China (21377008 and 21677004), National High Technology Research and Development Program (“863” Program) of China (2015AA034603), and Foundation of the Creative Research Team Construction Promotion Project of Beijing Municipal Institutions.

Appendix A. Supplementary data

Supplementary data associated with this article can be found, in the online version, at <http://dx.doi.org/10.1016/j.apcatb.2017.10.044>.

References

- X.T. Shen, L.H. Zhu, G.X. Liu, H.W. Yu, H.Q. Tang, Environ. Sci. Technol. 42 (2008) 1687–1692.
- X.Q. Sun, X.X. Xu, Appl. Catal. B 210 (2017) 149–159.
- G.D. Yang, Z. Jiang, H.H. Shi, T.C. Xiao, Z.F. Yan, J. Mater. Chem. 20 (2010) 5301–5309.
- Z.K. Zheng, B.B. Huang, X.Y. Qin, X.Y. Zhang, Y. Dai, M.-H. Whangbo, J. Mater. Chem. 21 (2011) 9079–9087.
- W. Wang, J.J. Fang, S.F. Shao, M. Lai, C.H. Lu, Appl. Catal. B 217 (2017) 57–64.
- C. Xue, X. Xu, G.D. Yang, S.J. Ding, RSC Adv. 5 (2015) 102228–102237.
- H.X. Li, Z.F. Bian, J. Zhu, Y.N. Huo, H. Li, Y.F. Lu, J. Am. Chem. Soc. 129 (2007) 4538–4539.
- N. Zhang, S.Q. Liu, X.Z. Fu, Y.J. Xu, J. Phys. Chem. C 115 (2011) 9136–9145.
- Y.B. Wang, X. Zhao, D. Cao, Y. Wang, Y.F. Zhu, Appl. Catal. B 211 (2017) 79–88.
- D.Q. Zhang, M.C. Wen, S.S. Zhang, P.J. Liu, W. Zhu, G.S. Li, H.X. Li, Appl. Catal. B 147 (2014) 610–616.
- X.C. Meng, Z.S. Zhang, Appl. Catal. B 209 (2017) 383–393.
- B.B. Chen, X.M. Li, R.J. Zheng, R.P. Chen, X. Sun, J. Mater. Chem. A 5 (2017) 13382–13391.
- Q. Kang, T. Wang, P. Li, L.Q. Liu, K. Chang, M. Li, J.H. Ye, Angew. Chem. Int. Ed. 54 (2015) 841–845.
- R. Su, R. Tiruvalam, Q. He, N. Dimitratos, L. Kesavan, C. Hammond, J.A. Lopez-Sanchez, R. Bechstein, C.J. Kiely, G.J. Hutchings, F. Besenbacher, ACS Nano 6 (2012) 6284–6292.
- R. Long, Y. Li, Y. Liu, S.M. Chen, X.S. Zheng, C. Gao, C.H. He, N.S. Chen, Z.M. Qi, L. Song, J. Jiang, J.F. Zhu, Y.J. Xiong, J. Am. Chem. Soc. 139 (2017) 4486–4492.
- H. Sudrajat, P. Sujaridworakun, J. Catal. 352 (2017) 394–400.
- H. Li, J. Shang, Z.H. Ai, L.Z. Zhang, J. Am. Chem. Soc. 137 (2015) 6393–6399.
- Q.F. Wu, S.Y. Bao, B.Z. Tian, Y.F. Xiao, J.L. Zhang, Chem. Commun. 52 (2016) 7478–7481.
- Y.Y. Zhu, Q. Ling, Y.F. Liu, H. Wang, Y.F. Zhu, Appl. Catal. B 187 (2016) 204–211.
- Y. Liu, L. Chen, Q. Yuan, J. He, C.T. Au, S.F. Yin, Chem. Commun. 52 (2016) 1274–1277.
- B. Zhang, J. Li, Y.Y. Gao, R.F. Chong, Z.L. Wang, L. Guo, X.W. Zhang, C. Li, J. Catal. 345 (2017) 96–103.
- Y. Park, K.J. McDonald, K.S. Choi, Chem. Soc. Rev. 42 (2013) 2321–2337.
- S.W. Cao, Z. Yin, J. Barber, F.Y.C. Boey, S.C.J. Loo, C. Xue, ACS Appl. Mater. Interfaces 4 (2012) 418–423.
- L. Ge, Mater. Chem. Phys. 107 (2008) 465–470.
- J.L. Zhang, Y. Lu, L. Ge, C.C. Han, Y.J. Li, Y.Q. Gao, S.S. Li, H. Xu, Appl. Catal. B 204 (2017) 385–393.
- W.G. Menezes, L. Altmann, V. Zielasek, K. Thiel, J. Catal. 300 (2013) 125–135.
- S.H. Xie, Y.X. Liu, J.G. Deng, X.T. Zhao, J. Yang, K.F. Zhang, Z. Han, H.X. Dai, J. Catal. 342 (2016) 17–26.
- X. Meng, L. Zhang, H.X. Dai, Z.X. Zhao, R.Z. Zhang, Y.X. Liu, Mater. Chem. Phys. 125 (2011) 59–65.
- K.F. Zhang, Y.X. Liu, J.G. Deng, S.H. Xie, H.X. Lin, X.T. Zhao, J. Yang, Z. Han, H.X. Dai, Appl. Catal. B 202 (2017) 569–579.
- R.C. Pawar, S. Kang, J.H. Park, J.H. Kim, S. Ahn, C.S. Lee, Catal. Sci. Technol. 7 (2017) 2579–2590.
- Y. Chang, K. Yu, C.X. Zhang, Z.Q. Yang, Y.J. Feng, H. Hao, Y.Z. Jiang, L.L. Lou, W.Z. Zhou, S.X. Liu, Appl. Catal. B 215 (2017) 74–84.
- S.B. Wang, X.C. Wang, Appl. Catal. B 162 (2015) 494–500.
- S.B. Wang, J.L. Lin, X.C. Wang, Phys. Chem. Chem. Phys. 16 (2014) 14656–14660.
- K.M. Mayer, J.H. Hafner, Chem. Rev. 111 (2011) 3828–3857.
- H.W. Huang, Y. He, X. Du, P.K. Chu, Y.H. Zhang, ACS Sustain. Chem. Eng. 3 (2015) 3262–3273.
- Y. Chang, K. Yu, C.X. Zhang, R. Li, P.Y. Zhao, L.L. Lou, S.X. Liu, Appl. Catal. B 176–177 (2015) 363–373.
- G. Darabdhara, P.K. Boruah, P. Borthakur, N. Hussain, M.R. Das, T. Ahamad, S.M. Alshehri, V. Malgras, K.C.-W. Wu, Y. Yamauchi, Nanoscale 8 (2016) 8276–8287.
- Y.X. Liu, H.X. Dai, J.G. Deng, L. Zhang, C.T. Au, Nanoscale 4 (2012) 2317–2325.
- H. Arandiyani, H.X. Dai, K.M. Ji, H.Y. Sun, J.H. Li, ACS Catal. 5 (2015) 1781–1793.
- Z. Wan, Q. Xu, H. Li, Y. Zhang, Y. Ding, J.D. Wang, Appl. Catal. B 210 (2017) 67–76.
- M.C. Long, W.M. Cai, J. Cai, B.X. Zhou, X.Y. Chai, Y.H. Wu, J. Phys. Chem. B 110 (2006) 20211–20216.
- J.N. Zhang, T.H. Chena, H.B. Lu, Z.B. Yang, F. Yin, J.Z. Gao, Q.R. Liu, Y.F. Tu, Appl. Surf. Sci. 404 (2017) 282–290.
- X.Z. Song, Q. Shi, H. Wang, S.L. Liu, C. Tai, Z.Y. Bian, Appl. Catal. B 203 (2017) 442–451.
- G.Q. Zhang, S.R. Sun, W.S. Jiang, X. Miao, Z. Zhao, X.Y. Zhang, D. Qu, D.Y. Zhang, D.B. Li, Z.C. Sun, Adv. Energy Mater. 7 (2017) 1600932.
- J.P. Zou, J. Ma, J.M. Luo, J. Yu, J.K. He, Y.T. Meng, Z. Luo, S.K. Bao, H.L. Liu, S.L. Luo, X.B. Luo, T.C. Chen, S.L. Suib, Appl. Catal. B 179 (2015) 220–228.
- H.W. Huang, X.W. Li, J.J. Wang, F. Dong, P.K. Chu, T.R. Zhang, Y.H. Zhang, ACS Catal. 5 (2015) 4094–4103.
- R.G. Li, H.X. Han, F.X. Zhang, D.E. Wang, C. Li, Energy Environ. Sci. 7 (2014) 1369–1376.
- Z.C. Lian, W.C. Wang, G.S. Li, F.H. Tian, K.S. Schanze, H.X. Li, ACS Appl. Mater. Interfaces 9 (2017) 16959–16966.
- S. Södergren, A. Hagfeldt, J. Olsson, S.-E. Lindquist, J. Phys. Chem. 98 (1994) 5552–5556.
- W.J. Jo, J.-W. Jang, K.-J. Kong, H.J. Kang, H.J. Kim, J.S. Lee, Angew. Chem. Int. Ed. 51 (2012) 3147–3151.
- Z. Wei, Y.F. Liu, J. Wang, R.L. Zong, W.Q. Yao, J. Wang, Y.F. Zhu, Nanoscale 7 (2015) 13943–13950.
- J. Wang, Y. Xia, H.Y. Zhao, G.D. Wang, L. Xiang, J.L. Xu, S. Komarneni, Appl. Catal. B 206 (2017) 406–416.
- K. Li, S.M. Gao, Q.Y. Wang, H. Xu, Z.Y. Wang, B.B. Huang, Y. Dai, J. Lu, ACS Appl. Mater. Interfaces 7 (2015) 9023–9030.
- E. Grabowska, M. Marchelek, T. Klimczuk, W. Lisowski, A. Zaleska-Medynska, J. Catal. 350 (2017) 159–173.